

**Nuclear antishadowing in neutrino deep inelastic scattering**Stanley J. Brodsky,<sup>1,\*</sup> Ivan Schmidt,<sup>2,†</sup> and Jian-Jun Yang<sup>2,3,4,‡</sup><sup>1</sup>*Stanford Linear Accelerator Center, Stanford University, Stanford, California 94309, USA*<sup>2</sup>*Departamento de Física, Universidad Técnica Federico Santa María, Casilla 110-V Valparaíso, Chile*<sup>3</sup>*Institut für Theoretische Physik, Universität Regensburg, D-93040 Regensburg, Germany*<sup>4</sup>*Department of Physics, Nanjing Normal University, Nanjing 210097, China*

(Received 21 September 2004; published 2 December 2004)

The shadowing and antishadowing of nuclear structure functions in the Gribov-Glauber picture is due, respectively, to the destructive and constructive interference of amplitudes arising from the multiple scattering of quarks in the nucleus. The effective quark-nucleon scattering amplitude includes Pomeron and Odderon contributions from multigluon exchange as well as Reggeon quark-exchange contributions. We show that the coherence of these multiscattering nuclear processes leads to shadowing and antishadowing of the electromagnetic nuclear structure functions in agreement with measurements. This picture leads to substantially different antishadowing for charged and neutral current reactions, thus affecting the extraction of the weak-mixing angle  $\theta_w$ . We find that part of the anomalous NuTeV result for  $\theta_w$  could be due to the nonuniversality of nuclear antishadowing for charged and neutral currents. Detailed measurements of the nuclear dependence of individual quark structure functions are thus needed to establish the distinctive phenomenology of shadowing and antishadowing and to make the NuTeV results definitive.

DOI: 10.1103/PhysRevD.70.116003

PACS numbers: 11.80.La, 13.15.+g, 25.30.Pt

**I. INTRODUCTION**

The precise determination of the weak-mixing angle  $\sin^2\theta_w$  plays a crucial role in testing the standard model of electroweak interactions. Until recently, a consistent value was obtained from all of the electroweak observables [1]. However, the NuTeV Collaboration [2] has determined a value for  $\sin^2\theta_w$  from measurements of the ratio of charged and neutral current deep inelastic neutrino-nucleus and antineutrino-nucleus scattering in iron targets which has a  $3\sigma$  deviation with respect to the fit of the standard model predictions from other electroweak measurements [1]. This contrasts with the recent determination of  $\sin^2\theta_w$  from parity violation in Möller scattering which is consistent with the standard model [3]. Although the NuTeV analysis takes into account many sources of systematic errors, there still remains the question of whether the reported deviation could be accounted for by QCD effects such as the asymmetry of the strange-antistrange quark sea [4,5] or other Standard Model effects [6–16]. In this paper we shall investigate whether the anomalous NuTeV result for  $\sin^2\theta_w$  could be due to the different behavior of leading twist nuclear shadowing and antishadowing effects for charged and neutral currents.

The physics of the nuclear shadowing in deep inelastic scattering can be most easily understood in the laboratory frame using the Glauber-Gribov picture [17,18]. The virtual photon,  $W$  or  $Z^0$  produces a quark-antiquark color-dipole pair which can interact diffractively or inelasti-

cally on the nucleons in the nucleus. The destructive interference of diffractive amplitudes from Pomeron exchange on the upstream nucleons then causes shadowing of the virtual photon interactions on the back face nucleons [19–24]. As emphasized by Ioffe [21], the coherence between processes which occur on different nucleons at separation  $L_A$  requires small Bjorken  $x_B$ :  $1/Mx_B = 2\nu/Q^2 \geq L_A$ . The coherence between different quark processes is also the basis of saturation phenomena in deep inelastic scattering (DIS) and other hard QCD reactions at small  $x_B$  [25], and coherent multiple parton scattering has been used in the analysis of  $p + A$  collisions in terms of the perturbative QCD factorization approach [26]. An example of the interference of one- and two-step processes in deep inelastic lepton-nucleus scattering is illustrated in Fig. 1.

An important aspect of the shadowing phenomenon is that the diffractive contribution  $\gamma^*N \rightarrow XN'$  to deep inelastic scattering (DDIS) where the nucleon  $N_1$  in Fig. 1 remains intact is a constant fraction of the total DIS rate, confirming that it is a leading-twist contribution. The Bjorken scaling of DDIS has been observed at HERA [27–29]. As shown in Ref. [30], the leading-twist contribution to DDIS arises in QCD in the usual parton model frame when one includes the nearly instantaneous gluon exchange final-state interactions of the struck quark with the target spectators. The same final-state interactions also lead to leading-twist single-spin asymmetries in semi-inclusive DIS [31]. Thus the shadowing of nuclear structure functions is also a leading-twist effect.

It was shown in Ref. [32] that if one allows for Reggeon exchanges which leave a nucleon intact, then one can

\*Email: sjbth@SLAC.Stanford.EDU

†Email: ivan.schmidt@fis.usm.cl

‡Deceased

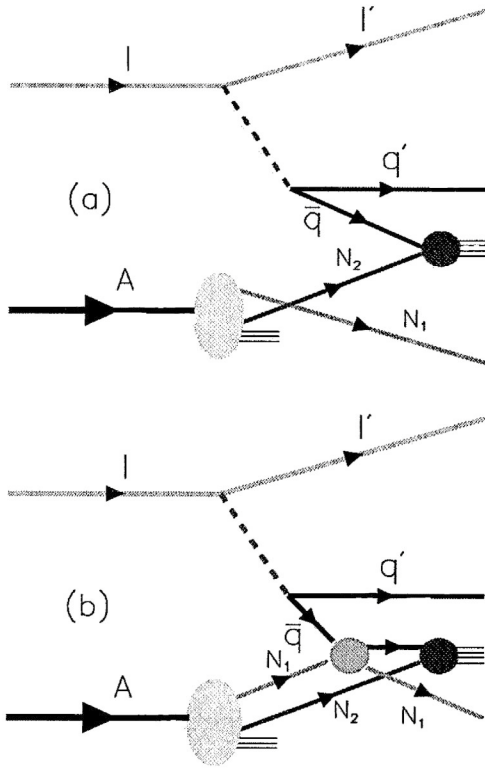


FIG. 1. The one-step (a) and two-step (b) processes in DIS on a nucleus. If the scattering on nucleon  $N_1$  is via Pomeron exchange, the one-step and two-step amplitudes are opposite in phase, thus diminishing the  $\bar{q}$  flux reaching  $N_2$ . This causes shadowing of the charge and neutral current nuclear structure functions.

obtain *constructive* interference among the multiscattering amplitudes in the nucleus. A Bjorken scaling contribution to DDIS from Reggeon exchange has in fact also been observed at HERA [28,29]. The strength and energy dependence of the  $C = +$  Reggeon  $t$ -channel exchange contributions to virtual Compton scattering is constrained by the Kuti-Weisskopf [33] behavior  $F_2(x) \sim x^{1-\alpha_R}$  of the nonsinglet electromagnetic structure functions at small  $x$ . The phase of the Reggeon exchange amplitude is determined by its signature factor. Because of this complex phase structure [32], one obtains constructive interference and *antishadowing* of the nuclear structure functions in the range  $0.1 < x < 0.2$ —a pronounced excess of the nuclear cross section with respect to nucleon additivity [34].

In the case where the diffractive amplitude on  $N_1$  is imaginary, the two-step process has the phase  $i \times i = -1$  relative to the one-step amplitude, producing destructive interference. (The second factor of  $i$  arises from integration over the quasireal intermediate state.) In the case where the diffractive amplitude on  $N_1$  is due to  $C = +$  Reggeon exchange with intercept  $\alpha_R(0) = 1/2$ , for example, the phase of the two-step amplitude in  $\frac{1}{\sqrt{2}}(1 - i) \times$

$i = \frac{1}{\sqrt{2}}(i + 1)$  relative to the one-step amplitude, thus producing constructive interference and antishadowing. This is discussed in more detail in the following sections.

Odderon exchange due to three-gluon exchange leads to an elastic quark-nucleon amplitude which is nearly real in phase, thus providing an additional mechanism for antishadowing. We shall show that the combination of Pomeron, Reggeon, and Odderon exchanges in multistep processes leads to shadowing and antishadowing of the electromagnetic nuclear structure functions in agreement with measurement in electromagnetic interactions. Shadowing of the nuclear structure functions is thus due to the dynamics of  $\gamma^*A$  interactions; it is not a property of the nuclear light-front wave function computed in isolation [30].

Evidence for the Odderon has been illusive; a detailed discussion can be found in a recent review by Ewerz [35]. A clear signal appears in the difference of proton-proton vs proton-antiproton scattering. From the perspective of QCD, the Odderon represents the color-singlet effects of three gluons in the  $t$ -channel. A general treatment in the context of the BFKL program has been given by Bartels, Lipatov, and Vacca [36]. The Odderon has Regge intercept  $\alpha_O \sim 1$ ,  $C = -$ , and thus its phase is nearly pure real. The Odderon does not contribute directly to the structure functions since it gives real contribution to the virtual Compton amplitude. However, it can play an important role in the multiscattering series in the nuclear target.

There can be other important antishadowing mechanisms. Processes which can occur on a nucleus, but are forbidden on a nucleon, will enhance the nuclear structure functions. For example, pseudoscalar Reggeon exchange amplitudes do not contribute to DIS on a nucleon target since the helicity-conserving forward amplitude  $\gamma^*N \rightarrow \gamma^*N$  vanishes at  $t = 0$ . However in the nuclear case, the interactions of the scattered quark (due to Pomeron exchange) on a second nucleon  $N_2$  in a nuclear target can skew the kinematics of  $\gamma^*N_1 \rightarrow \gamma^*N'_1$ , thus allowing the pseudoscalar exchange to occur on the nucleon  $N_1$  at  $t \neq 0$ . This also requires nonzero orbital angular momentum of the nucleons in the nuclear wave function. Notice that the virtual Compton amplitude on the nucleus  $\gamma^*A \rightarrow \gamma^*A$  is still evaluated at zero momentum transfer  $t = 0$ . Thus in general one should include pseudoscalar exchange in the parametrization of the quark multiple scattering processes.

In Fig. 2 we illustrate several leading-twist QCD contributions to the nuclear structure function as calculated from the absorptive part of the forward virtual Compton amplitude  $ImT(\gamma^*A \rightarrow \gamma^*A)$ , in the  $q^+ = 0$ ,  $q_\perp^2 = Q^2$  parton model frame and in the laboratory frame where  $q^+ > 0$ . Notice the final-state two-gluon exchange “Pomeron” interaction of the outgoing quark on a target neutron. Figure 2(c) is an illustration of a doubly inelastic discontinuity of the same two-step process as (a) in the

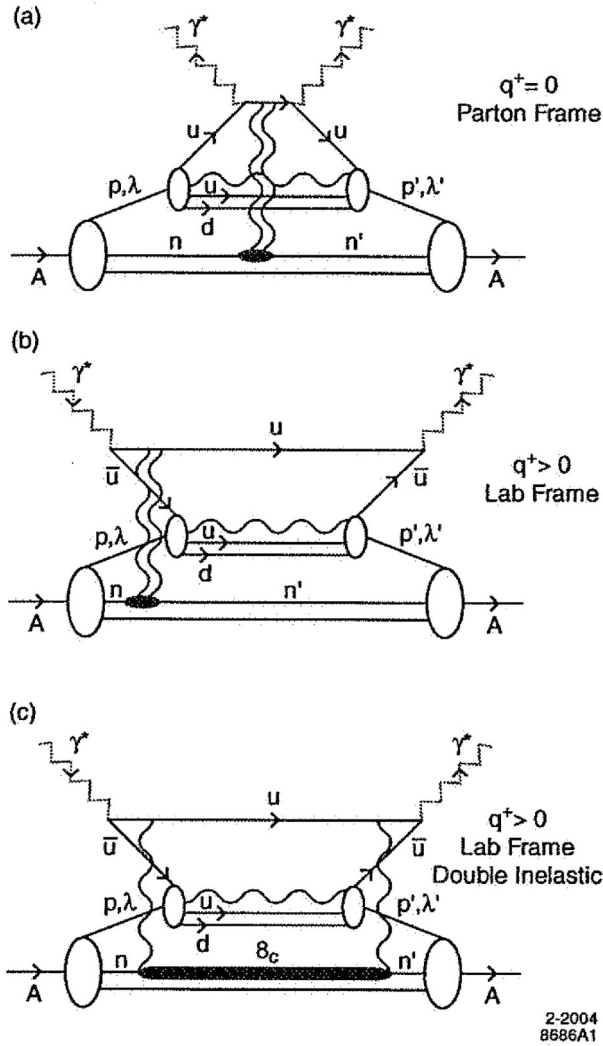


FIG. 2. Representation of leading-twist QCD contributions to the nuclear structure function as calculated from the absorptive part of the forward virtual Compton amplitude  $ImT(\gamma^*A \rightarrow \gamma^*A)$ . (a) Illustration of a two-step contribution in the usual  $q^+ = 0$ ,  $a_\perp^2 = Q^2$  parton model frame. The deep inelastic scattering of a lepton on a valence quark of a target proton is followed by the final-state two-gluon exchange Pomeron interaction of the outgoing quark on a neutron. (b) Illustration of the physics of the same two-step process illustrated in (a), but in the laboratory frame where  $q^+ > 0$ . The  $u\bar{u}$  fluctuation of the virtual photon scatters elastically via two-gluon exchange on a neutron; this is then followed by the annihilation of the  $\bar{u}$  quark on a proton. (c) Illustration of a doubly inelastic discontinuity of the same two-step process as (a) in the laboratory frame  $q^+ > 0$ . The  $u\bar{u}$  fluctuation of the virtual photon first scatters inelastically on a neutron via a single-gluon exchange which produces an excited color state  $8_C$  of the neutron. This is then followed by the annihilation of the  $\bar{u}$  quark on a proton.

laboratory frame  $q^+ > 0$ . The  $u\bar{u}$  fluctuation of the virtual photon first scatters inelastically on a neutron via a single-gluon exchange which produces an excited color state  $8_C$  of the neutron. This is then followed by the

annihilation of the  $\bar{u}$  quark on a proton. The two-step amplitudes of (b) or (c) will interfere destructively with the single-step annihilation amplitude on the proton alone, thus producing shadowing. If the proton spin  $S_z^p$  is flipped ( $\lambda' \neq \lambda$ ) by the valence interaction, as occurs in pseudoscalar Reggeon exchange, then the single-step process cannot contribute to the forward virtual Compton amplitude, and the two-step process itself produces antishadowing of the valence quark distributions. Similar processes occur in the case of the electroweak currents.

Figure 3 illustrates a similar situation, but for the three-gluon ‘‘Odderon’’ exchange. In this case, the two-step amplitudes of (b) or (c) can interfere constructively with the Regge-behaved single-step annihilation amplitude on the proton alone, thus producing antishadowing. Similar processes occur in the case of the electroweak currents.

The Reggeon contributions to the quark scattering amplitudes depend specifically on the quark flavor; for example, the isovector Regge trajectories couple differently to  $u$  and  $d$  quarks. The  $s$  and  $\bar{s}$  couple to yet different Reggeons. This implies distinct antishadowing effects for each quark and antiquark component of the nuclear structure function; this in turn implies nonuniversality of antishadowing of the charged, neutral, and electromagnetic current. Antineutrino and neutrino reactions will also have different antishadowing effects. In addition, there is another source of antishadowing, specific to non-Abelian theories, which is discussed in more detail in the appendix. It includes one-gluon exchange  $\times$  Reggeon exchange, assuming the existence of hidden-color components in the nuclear wave function. We do not explicitly include this effect in our analysis since the parametrization is uncertain.

There are also antishadowing contributions arising from two-step processes involving Reggeon  $\times$  Reggeon exchange, but these contributions are power-law suppressed in the Bjorken limit. We will not include these higher-twist effects in our analysis.

In this paper we shall show in detail that the Gribov-Glauber picture for nuclear deep inelastic scattering leads to substantially different nuclear effects for charged and neutral currents; in fact, the neutrino and antineutrino cross sections are each modified in substantially different ways due to the various allowed Regge exchanges. This nonuniversality of nuclear effects will modify the extraction of the weak-mixing angle  $\sin^2\theta_W$  obtained from the ratio of charged and neutral current deep inelastic neutrino-nucleus scattering.

## II. NUCLEAR SHADOWING AND ANTISHADOWING EFFECTS DUE TO MULTIPLE SCATTERING

In this section, we will extend the analysis of Ref. [32] for the electromagnetic interaction case to the neutrino

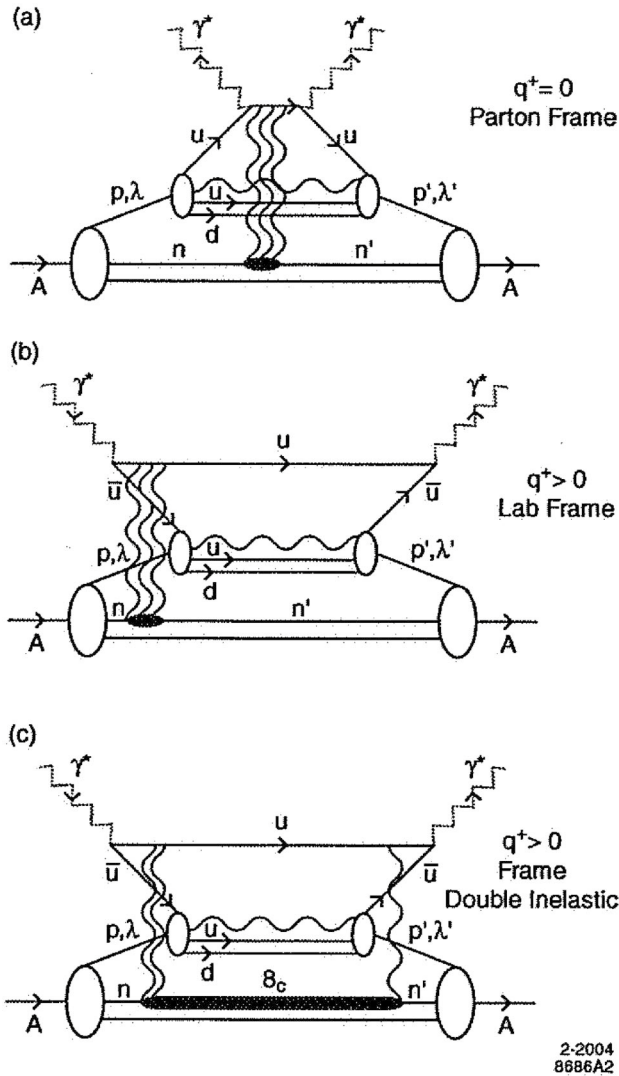


FIG. 3. Representation of leading-twist QCD contributions to the nuclear structure function from the absorptive part of the forward virtual Compton amplitude  $ImT(\gamma^*A \rightarrow \gamma^*A)$  involving Odderon exchange. (a) Illustration of a two-step contribution in the  $q^+ = 0$ ,  $q_\perp^2 = Q^2$  parton model frame—deep inelastic lepton scattering on a valence quark of a target proton followed by the final-state three-gluon exchange Odderon interaction of the outgoing quark on a target neutron. (b) Illustration of the physics of the same two-step process shown in (a), but in the laboratory frame where  $q^+ > 0$ . The  $u\bar{u}$  fluctuation of the virtual photon first scatters elastically via three-gluon exchange on a neutron; this is then followed by the annihilation of the  $\bar{u}$  quark on a proton. (c) Illustration of a doubly inelastic discontinuity of the same two-step process as (a) in the laboratory frame  $q^+ > 0$ . The  $u\bar{u}$  fluctuation of the virtual photon first scatters inelastically on a neutron via two-gluon exchange which produces an excited color state  $\delta_c$  of the neutron. This is then followed by the annihilation of the  $\bar{u}$  quark on a proton. The two-step amplitudes of (b) or (c) can interfere constructively with the Regge-behaved single-step annihilation amplitude on the proton alone, thus producing antishadowing. Similar processes occur in the case of the electroweak currents.

DIS case. The general approach is based on the “covariant parton model” [37,38], which provides a relationship of deep inelastic cross section to quark-nucleon scattering. The central idea is the following: In neutrino DIS on a nucleus  $A$ , although the virtual current may interact inelastically with a nucleon coming from the nucleus in a one-step process as shown in Fig. 1(a), it can also interact elastically with several nucleons before the final nucleon interacts inelastically as depicted in Fig. 1(b). The interacting antiquark of quark is spacelike:

$$\tau^2 = -k^2 = x(s + k_\perp^2)/(1 - x) - xM^2 + k_\perp^2 \quad (1)$$

is the negative of the invariant momentum squared of the interacting parton. Here  $M = \frac{1}{2}(M_p + M_n)$  is the nucleon mass, and  $k_\perp$  is the parton’s transverse momentum. The quark-nucleon amplitude is assumed to be damped at large quark virtuality  $\tau$ , so that the quark-nucleon invariant  $s = (k + p)^2$  grows as  $1/x$ . This description of deep inelastic scattering is consistent with recent analysis of the role of final-state gluon interactions in QCD when one chooses light cone gauge to make the Wilson line integral vanish [30].

At high energies the phase of the elastic amplitude is approximately imaginary since it corresponds to Pomeron exchange. The accumulated phase in multiple scattering is also imaginary. Therefore, the two-step amplitude is coherent and opposite in phase to the one-step amplitude where the beam interacts directly on  $N_2$  without initial-state interactions; the target nucleon  $N_2$  feels less incoming flux, which results in nuclear shadowing. Since there may be an  $\alpha_R$  Reggeon or Odderon contribution to the  $\bar{q}N$  amplitude, the real phase introduced by such contributions leads to antishadowing effect. In this picture, antishadowing is attributed to a dynamical mechanism rather than being enforced to satisfy the momentum sum rule [39]. The sum rule can still be maintained by the nuclear modifications of the gluon distribution.

We now develop the detailed formulas which describe the nuclear shadowing and antishadowing effects.

### A. Parametrizations of quark-nucleon scattering

We shall assume that the high-energy antiquark-nucleon scattering amplitude  $T_{\bar{q}N}$  has the Regge and analytic behavior characteristic of normal hadronic amplitudes. Following the model of Ref. [32], we consider a standard Reggeon at  $\alpha_R = \frac{1}{2}$ , and Odderon exchange term, a pseudoscalar exchange term, and a term at  $\alpha_R = -1$ , in addition to the Pomeron-exchange term.

The Pomeron exchange has the intercept  $\alpha_P = 1 + \delta$ . For the amputated  $\bar{q} - N$  amplitude  $T_{\bar{q}N}$  and  $q - N$  amplitude  $T_{qN}$  with  $q = u$  and  $d$ ,  $N = p$  and  $n$ , we assume the following parametrizations, including terms which represent pseudoscalar Reggeon exchange. Then resulting amplitudes are:

$$\begin{aligned}
 T_{\bar{u}-p} = & \sigma \left[ s \left( i + \tan \frac{\pi \delta}{2} \right) \beta_1(\tau^2) - s \beta_O(\tau^2) \right. \\
 & - (1-i)s^{1/2} \beta_{1/2}^{0+}(\tau^2) + (1+i)s^{1/2} \beta_{1/2}^{0-}(\tau^2) \\
 & - (1-i)s^{1/2} \beta_{1/2}^{1+}(\tau^2) + W(1-i)s^{1/2} \beta_{1/2}^{\text{pseudo}}(\tau^2) \\
 & \left. + (1+i)s^{1/2} \beta_{1/2}^{1-}(\tau^2) + is^{-1} \beta_{-1}^u(\tau^2) \right], \quad (2)
 \end{aligned}$$

$$\begin{aligned}
 T_{\bar{d}-p} = & \sigma \left[ s \left( i + \tan \frac{\pi \delta}{2} \right) \beta_1(\tau^2) - s \beta_O(\tau^2) \right. \\
 & - (1-i)s^{1/2} \beta_{1/2}^{0+}(\tau^2) + (1+i)s^{1/2} \beta_{1/2}^{0-}(\tau^2) \\
 & + (1-i)s^{1/2} \beta_{1/2}^{1+}(\tau^2) + W(1-i)s^{1/2} \beta_{1/2}^{\text{pseudo}}(\tau^2) \\
 & \left. - (1+i)s^{1/2} \beta_{1/2}^{1-}(\tau^2) + is^{-1} \beta_{-1}^d(\tau^2) \right], \quad (3)
 \end{aligned}$$

$$\begin{aligned}
 T_{u-p} = & \sigma \left[ s \left( i + \tan \frac{\pi \delta}{2} \right) \beta_1(\tau^2) + s \beta_O(\tau^2) \right. \\
 & - (1-i)s^{1/2} \beta_{1/2}^{0+}(\tau^2) - (1+i)s^{1/2} \beta_{1/2}^{0-}(\tau^2) \\
 & - (1-i)s^{1/2} \beta_{1/2}^{1+}(\tau^2) + W(1-i)s^{1/2} \beta_{1/2}^{\text{pseudo}}(\tau^2) \\
 & \left. - (1+i)s^{1/2} \beta_{1/2}^{1-}(\tau^2) \right], \quad (4)
 \end{aligned}$$

$$\begin{aligned}
 T_{d-p} = & \sigma \left[ s \left( i + \tan \frac{\pi \delta}{2} \right) \beta_1(\tau^2) + s \beta_O(\tau^2) \right. \\
 & - (1-i)s^{1/2} \beta_{1/2}^{0+}(\tau^2) - (1+i)s^{1/2} \beta_{1/2}^{0-}(\tau^2) \\
 & + (1-i)s^{1/2} \beta_{1/2}^{1+}(\tau^2) + W(1-i)s^{1/2} \beta_{1/2}^{\text{pseudo}}(\tau^2) \\
 & \left. + (1+i)s^{1/2} \beta_{1/2}^{1-}(\tau^2) \right], \quad (5)
 \end{aligned}$$

$$\begin{aligned}
 T_{\bar{u}-n} = & \sigma \left[ s \left( i + \tan \frac{\pi \delta}{2} \right) \beta_1(\tau^2) - s \beta_O(\tau^2) \right. \\
 & - (1-i)s^{1/2} \beta_{1/2}^{0+}(\tau^2) + (1+i)s^{1/2} \beta_{1/2}^{0-}(\tau^2) \\
 & + (1-i)s^{1/2} \beta_{1/2}^{1+}(\tau^2) + W(1-i)s^{1/2} \beta_{1/2}^{\text{pseudo}}(\tau^2) \\
 & \left. - (1+i)s^{1/2} \beta_{1/2}^{1-}(\tau^2) + is^{-1} \beta_{-1}^d(\tau^2) \right], \quad (6)
 \end{aligned}$$

$$\begin{aligned}
 T_{\bar{d}-n} = & \sigma \left[ s \left( i + \tan \frac{\pi \delta}{2} \right) \beta_1(\tau^2) - s \beta_O(\tau^2) \right. \\
 & - (1-i)s^{1/2} \beta_{1/2}^{0+}(\tau^2) + (1+i)s^{1/2} \beta_{1/2}^{0-}(\tau^2) \\
 & - (1-i)s^{1/2} \beta_{1/2}^{1+}(\tau^2) + W(1-i)s^{1/2} \beta_{1/2}^{\text{pseudo}}(\tau^2) \\
 & \left. + (1+i)s^{1/2} \beta_{1/2}^{1-}(\tau^2) + is^{-1} \beta_{-1}^u(\tau^2) \right], \quad (7)
 \end{aligned}$$

$$\begin{aligned}
 T_{u-n} = & \sigma \left[ s \left( i + \tan \frac{\pi \delta}{2} \right) \beta_1(\tau^2) + s \beta_O(\tau^2) \right. \\
 & - (1-i)s^{1/2} \beta_{1/2}^{0+}(\tau^2) - (1+i)s^{1/2} \beta_{1/2}^{0-}(\tau^2) \\
 & + W(1-i)s^{1/2} \beta_{1/2}^{\text{pseudo}}(\tau^2) + (1-i)s^{1/2} \beta_{1/2}^{1+}(\tau^2) \\
 & \left. + (1+i)s^{1/2} \beta_{1/2}^{1-}(\tau^2) \right], \quad (8)
 \end{aligned}$$

$$\begin{aligned}
 T_{d-n} = & \sigma \left[ s \left( i + \tan \frac{\pi \delta}{2} \right) \beta_1(\tau^2) + s \beta_O(\tau^2) \right. \\
 & - (1-i)s^{1/2} \beta_{1/2}^{0+}(\tau^2) - (1+i)s^{1/2} \beta_{1/2}^{0-}(\tau^2) \\
 & - (1-i)s^{1/2} \beta_{1/2}^{1+}(\tau^2) + W(1-i)s^{1/2} \beta_{1/2}^{\text{pseudo}}(\tau^2) \\
 & \left. - (1+i)s^{1/2} \beta_{1/2}^{1-}(\tau^2) \right]. \quad (9)
 \end{aligned}$$

$W = 0$  and  $1$ , since the pseudoscalar term cannot act just once in the multiple scattering.

Here

$$\beta_j(\tau^2) = \frac{f_j}{1 + (\tau^2/\bar{v}_j^2)^{n_j}}, \quad (10)$$

with  $j = 1, 1/2, -1, O$ , and *pseudo* (pseudoscalar). The parameters  $n_j$  ( $j = 1, 1/2$ , and  $-1$ ) are taken to be the same as those in Ref. [32]. [See also Table I.]

The odd-C Odderon with  $\alpha_O = 1$  has a real coupling compared to the imaginary coupling of the even C Pomeron. It reduces nuclear shadowing and produces antishadowing although it does not contribute to the free nucleon structure functions. In the following numerical estimate, we take  $f_O = 0.1$ . In order to fit the large  $x$  experimental data on the parton distributions of the nucleon, we introduce different values for the parameters  $\bar{v}_{-1}^2$  which control the off shell dependence of the  $\bar{q} - N$  amplitudes. We denote them as  $\bar{v}_{-1}^{(u)2}$  and  $\bar{v}_{-1}^{(d)2}$  for the  $u$  and  $d$  quarks, respectively.

We take the overall amplitude strength  $\sigma$  to be the same in all cases, with a value:

$$\sigma = 66 \text{ mb}. \quad (11)$$

The  $I = 1$  Reggeon terms in the amplitudes play a very important role, reflecting the sea asymmetry  $\bar{d} - \bar{u}$  of the nucleon in the low  $x$  region.

In principle,  $I = 1$  pseudoscalar exchange should also contribute here, but the  $\gamma * A \rightarrow \gamma * A$  cross section is not sensitive to its parameters, and therefore its strength cannot be fixed. Careful fits to deeply virtual Compton scattering (DVCS) and other processes sensitive to the  $I = 1$  pseudoscalar exchanges are needed. The  $I = 0$  coupling is constrained by our fit to antishadowing for electromagnetic DIS. Then we can predict antishadowing for weak DIS.

TABLE I. Parameters in our numerical calculation.

$\bar{v}_1^2$	0.2 GeV <sup>2</sup>	$f_1, f_1^s$	1.0, 0.5
$\bar{v}_{1/2}^2$	0.2 GeV <sup>2</sup>	$f_{1/2}^{0+}, f_{1/2}^{0-}, f_{1/2}^{1+}, f_{1/2}^{1-}$	0.30, 0.3, 0.1, 0.3 GeV
$\bar{v}_{-1}^{(u)2}, \bar{v}_{-1}^{(d)2}$	1.3, 0.65 GeV <sup>2</sup>	$f_{-1}$	0.45 GeV <sup>4</sup>
$\bar{v}_0^2$	0.30 GeV <sup>2</sup>	$f_0$	0.10
$\bar{v}_p^2$	1.0 GeV <sup>2</sup>	<b>b</b>	10 (GeV/c) <sup>-2</sup>
$\sigma$	66 mb	$n_{-1}$	2
$f_{\text{pseudo}}$	1.35 GeV	$n_1, n_{1/2}, n_0$	4

In principle, each Reggeon in the model of  $qN$  scattering amplitude should couple to the individual quarks with the appropriate isospin and charge conjugation dependence. For example, the  $\rho$  Reggeon couples as an  $I = 1$ ,  $C = -$  exchange. Although Reggeons of both  $C = \pm$  appear in the quark-nucleon amplitude, in the end after multiple interactions and summing over quark and anti-quark currents, the nuclear Compton amplitude has only  $C = +$  exchange in the  $t$ -channel. In our model, the Reggeon term in the  $q - N$  amplitude with  $I = 0$  and  $C = +$  is taken to represent the sum of the possible Reggeon exchanges. At leading twist only the Pomeron and Odderon which derive from gluon exchange survive in the multiple scattering. The Reggeon exchange to elastic scattering in the multiple scattering is suppressed.

In the present analysis, we also include the strange quark contribution. The antistrange quark can scatter elastically on one nucleon via Pomeron, Odderon, and  $\phi$  Reggeon exchanges. The Reggeon intercept for the  $\phi$  trajectory is close to  $\alpha_R(0) \sim 0$  since  $\alpha_R(m_\phi^2) = 1$  and the Regge slope is universal. Actually, the  $\phi$  trajectory can be parametrized as  $\alpha_R(t) = 0.1 + 0.9t$  [40]. Then we can parametrize the amputated  $\bar{s} - N$  and  $s - N$  amplitudes as:

$$T_{\bar{s}-N} = \sigma_{\bar{s}-N} \{ i s \beta_1^{(s)}(\tau^2) - s \beta_0^{(s)}(\tau^2) + s^{0.1} [(1 + \cos 0.1\pi) - i \sin 0.1\pi] \beta_{0.1}(\tau^2) \}, \quad (12)$$

$$T_{s-N} = \sigma_{s-N} \{ i s \beta_1^{(s)}(\tau^2) + s \beta_0^{(s)}(\tau^2) + s^{0.1} [(1 + \cos 0.1\pi) - i \sin 0.1\pi] \beta_{0.1}(\tau^2) \}, \quad (13)$$

where  $\sigma_{\bar{s}-N} = \sigma_{s-N} = \sigma$  and  $N = p$  and  $n$ . Since the Pomeron coupling to the strange quark could be less in strength than its coupling to light quarks,  $f_1^{(s)}$  should be smaller than  $f_1 = 1$  for  $u$  and  $d$  quarks. We take  $f_1^{(s)} = 0.1$ . The value of the Reggeon coupling  $f_{0.1}$  in  $\beta_{0.1}(\tau^2)$  is taken as  $0.2 \text{ GeV}^{0.9}$ , which is the suitable mass dimension in order to have the proper mass dimension of the Reggeon terms. With the above choice of the parameters, we can produce a shape of strange quark distributions which is close to those obtained by a fit analysis [41],

CTEQ-5 parametrization [42], and MRST parametrization [43].

If we use  $N = p$  and  $n$ , indicating a proton and neutron target, respectively, then for an isoscalar target  $N_0$ , the amplitude  $T_{\bar{q}N_0}$  per nucleon is

$$T_{\bar{q}N_0} = \frac{1}{2} (T_{\bar{q}p} + T_{\bar{q}n}). \quad (14)$$

Then we introduce

$$T_{N_0}(s, \tau^2) = T_{\bar{q}N_0}(s, \tau^2) \Delta_F^2(\tau^2), \quad (15)$$

and

$$i \Delta_F(\tau^2) \sim \frac{1}{\bar{v}_p^2 + \tau^2}. \quad (16)$$

Now let us turn to the scattering on a nuclear ( $A$ ) target. We expect that the  $\bar{q} - A$  scattering amplitude can be obtained from the  $\bar{q} - N$  amplitude according to Glauber's theory as follows,<sup>1</sup>

$$T_{\bar{q}A} = \sum_{k_1=0}^Z \sum_{k_2=0}^N \frac{1}{k_1 + k_2} \binom{Z + N}{k_1 + k_2} \frac{1}{M} \alpha^{k_1 + k_2 - 1} (T_{\bar{q}p})^{k_1} \times (T_{\bar{q}n})^{k_2} \theta(k_1 + k_2 - 1), \quad (17)$$

where

$$M = \min\{k_1 + k_2, Z\} - \max\{k_1 + k_2 - N, 0\} + 1 \\ = \min\{k_1 + k_2, N\} - \max\{k_1 + k_2 - Z, 0\} + 1 \quad (18)$$

and

$$\alpha = \frac{i}{4\pi p_{\text{c.m.}} s^{1/2} (R^2 + 2b)}, \quad (19)$$

with

<sup>1</sup>At high energies, long Ioffe distances  $L_I = \frac{2\nu}{Q^2}$ , where the longitudinal momentum transfer to a scattered nucleon is small compared to the inverse nuclear size, the one-step and two-step amplitudes can interfere. There is actually a relative phase factor  $\exp(-i\Delta k \cdot x)$  between the two processes, which can be ignored at small  $x_{bj}$ . This factor controls the coherence.

$$p_{c.m.} = \sqrt{\tau^2 + (s - M^2 - \tau^2)^2/4s}, \quad (20)$$

$$R^2 = \frac{2}{3}R_0^2, \quad R_0 = 1.123A^{1/3} \text{ fm}, \quad (21)$$

and  $b = 10 \text{ (GeV/c)}^{-2}$  is used [32]. Furthermore, we introduce

$$T_A(s, \tau^2) = T_{\bar{q}A}(s, \tau^2)\Delta_F^2(\tau^2). \quad (22)$$

Similar expressions hold for  $T_{qA}$ .

The Regge contribution to the deep inelastic cross section comes from the handbag contribution to the forward virtual Compton amplitude  $\gamma^*p \rightarrow \gamma^*p$ . The Regge behavior  $x^{-\alpha_R(0)}$  arises from the summation over higher Fock states. The phase of the  $I = 0$  Reggeon contribution  $(-i + 1)$  with  $\alpha_R = 1/2$  entering the virtual Compton amplitude is opposite to the positive imaginary contribution of Pomeron exchange and thus tends to reduce the deep inelastic cross section on a nucleon.

As shown in Ref. [30], the multiple scattering contributions from elastic scattering from Reggeon exchange is a higher-twist contribution to the deep inelastic cross section; only gauge interactions have a final state interactions (FSI) effect in the Bjorken limit [30]. The Pomeron and Odderon nominally have  $\alpha_O \simeq 1$ , so their contributions to elastic scattering are not suppressed in the Bjorken limit, since they are derived from multiple gluon exchange. Thus the Pomeron and Odderon can act any number of times in the nucleus, but the Reggeon can act only once at leading twist. In effect the Reggeon does not have enough time to form in the FSI at small invariant separation  $x^2 \sim 1/Q^2$ . Thus FSIs from Reggeons in  $T_{\bar{q}A}$  with  $\alpha_R \sim 0.5$  should be suppressed in the Bjorken limit by a power of  $1/Q$ . In order to implement this we put a suppression factor  $R_D$  in the multiple scattering Reggeon terms:

$$R_D = \left( \frac{Q_0^2}{Q_0^2 + Q^2} \right)^{1/2} \quad (23)$$

for the  $u$  and  $d$  quarks. And

$$R_D = \left( \frac{Q_0^2}{Q_0^2 + Q^2} \right) \quad (24)$$

for the  $s$  quark with  $Q_0^2 \simeq 1 \text{ GeV}^2$ , a typical hadronic scale.

When we take the limit of large  $Q^2$ , the antishadowing due to elastic Reggeon exchanges is quenched; however, the presence of the Odderon can produce antishadowing. For example, a two-step nuclear process shown in Fig. 3(b) from elastic Odderon scattering plus inelastic Reggeon scattering gives a contribution to the virtual Compton amplitude  $1 \times i \times (i + 1) = (-1 + i)$ . [The middle factor of  $i$  is due to the cut between the two steps.] The positive imaginary contribution to the two-step am-

plitude produces an enhancement of the nuclear cross section relative to the nucleon cross section in the regime  $x \sim 0.1$  where the Reggeon contribution to deep inelastic scattering is important. This is a key feature of our model. Note that the two-step process of Odderon plus Pomeron produces only a real contribution to the virtual Compton amplitude. The Pomeron-Pomeron and Pomeron-Reggeon two-step contributions reduce the one-step Pomeron plus Reggeon contributions, respectively, and thus only produce nuclear shadowing.

We can also consider the two-step  $[PiR_\pi]$  contribution to  $ImT_{\gamma^*A \rightarrow \gamma^*A}$ , which involves the imaginary part  $ImR_\pi$  of the (nonforward) pion Reggeon exchange amplitude. The pion pole term alone is real so we consider the pion Regge trajectory—the Reggeized version of pion exchange. When we take its absorptive part, we look at the cut through a  $q\bar{q}$  ladder exchanged on the second nucleon. Since the Reggeized pion exchange has  $I = 1$  and the Pomeron is  $I = 0$ , the two-step  $[PiR_\pi]$  contribution does not contribute to  $ImT_{\gamma^*A \rightarrow \gamma^*A}$  if the target is  $I = 0$ . Thus there is no antishadowing contribution from  $[PiR_\pi]$  to the deuteron structure function. However, there are other pseudoscalar exchanges possible, such as the  $\eta$  Reggeon.

It is interesting to analyze the situation from the point of view of angular momentum. The question is whether the two-step process  $[PiR_\pi]$  requires orbital angular momentum in the ground state nuclear wave function. Consider the  $[PiR_\pi]$  contribution to the forward virtual Compton amplitude  $ImT_{\gamma^*A \rightarrow \gamma^*A}$ . The Pomeron exchange on the first nucleon gives a transverse momentum kick  $\vec{k}_\perp$ . The pion Reggeon exchange on the second nucleon gives a balancing opposite kick  $-\vec{k}_\perp$  so that we can have a forward nuclear amplitude. The pseudoscalar exchange on the second nucleon is a  $\Delta L = 1$  transition. That is why the amplitude requires nonzero  $k_\perp$ . Thus we are actually looking at the overlap of nuclear Fock components of the nucleus with  $\Delta L = 1$ . This is the same admixture which in the spin-1/2 case gives a nuclear magnetic anomalous moment.

The unpolarized quark distribution functions in an isoscalar target ( $N_0$ ) and nucleus target ( $A$ ) are, respectively,

$$xq^{N_0}(x) = \frac{2}{(2\pi)^3} \frac{Cx^2}{1-x} \int ds d^2\mathbf{k}_\perp ImT_{N_0}(s, \mu^2), \quad (25)$$

$$xq^A(x) = \frac{2}{(2\pi)^3} \frac{Cx^2}{1-x} \int ds d^2\mathbf{k}_\perp ImT_A(s, \mu^2), \quad (26)$$

$$\mu^2 = -\tau^2. \quad (27)$$

The constant  $C$  is related to the parton wave function renormalization constant.

With the obtained quark distribution  $xq^{N_0(A)}(x)$  for an isoscalar target  $N_0$  or a nucleus target  $A$ , we can calculate the structure functions for various current exchanges.

### 1. The photon exchange case

$$F_1^{\gamma N_0(A)} = \frac{1}{2} \left[ \frac{4}{9} [u(x)^{N_0(A)} + \bar{u}^{N_0(A)}] + \frac{1}{9} [d(x)^{N_0(A)} + \bar{d}^{N_0(A)} + s(x)^{N_0(A)} + \bar{s}^{N_0(A)}] \right], \quad (28)$$

$$F_2^{\gamma N_0(A)} = 2xF_1^{\gamma N_0(A)}. \quad (29)$$

### 2. The neutral current exchange case

The structure functions of the neutral current (NC) reaction are

$$F_1^{ZN_0(A)} = \frac{1}{2} \left\{ [(g_V^u)^2 + (g_A^u)^2] [u^{N_0(A)}(x) + \bar{u}^{N_0(A)}(x)] + [(g_V^d)^2 + (g_A^d)^2] [d^{N_0(A)}(x) + \bar{d}^{N_0(A)}(x)] + s^{N_0(A)}(x) + \bar{s}^{N_0(A)}(x) \right\}, \quad (30)$$

$$F_2^{ZN_0(A)} = 2xF_1^{ZN_0(A)}, \quad (31)$$

$$F_3^{ZN_0(A)} = 2 \{ g_V^u g_A^u [u^{N_0(A)}(x) - \bar{u}^{N_0(A)}(x)] + g_V^d g_A^d [d^{N_0(A)}(x) - \bar{d}^{N_0(A)}(x)] + s^{N_0(A)}(x) - \bar{s}^{N_0(A)}(x) \}. \quad (32)$$

In the Standard Model (SM) the vector and axial-vector quark couplings are given by

$$g_V^u = \frac{1}{2} - \frac{4}{3} \sin^2 \theta_W, \quad g_V^d = -\frac{1}{2} + \frac{2}{3} \sin^2 \theta_W, \\ g_A^u = \frac{1}{2}, \quad g_A^d = -\frac{1}{2},$$

where  $\sin^2 \theta_W$  is the weak-mixing angle.

### 3. The charged current exchange case

The structure function of the charged current (CC) reaction is given by

$$F_1^{W^+ N_0(A)} = \bar{u}^{N_0(A)}(x) (|V_{ud}|^2 + |V_{us}|^2) + \bar{u}^{N_0(A)}(\xi_b) |V_{ub}|^2 \theta(x_b - x) + d^{N_0(A)}(x) |V_{ud}|^2 + d^{N_0(A)}(\xi_c) |V_{cd}|^2 \theta(x_c - x) + s^{N_0(A)}(x) |V_{us}|^2 + s^{N_0(A)}(\xi_c) |V_{cs}|^2 \theta(x_c - x), \quad (33)$$

here  $V_{ij}$  are the Cabibbo-Kobayashi-Maskawa mixing matrix elements. The variable

$$\xi_k = \begin{cases} x \left( 1 + \frac{m_k^2}{Q^2} \right), & (k = c, b), \\ x, & (k = u, d, s) \end{cases}$$

and the step functions  $\theta(x_c - x)$ ,  $\theta(x_b - x)$  take into account rescaling due to heavy quark production thresholds.

The structure functions  $F_2^{W^+ N_0(A)}$  and  $F_3^{W^+ N_0(A)}$  are obtained from (33) by the replacement of the quark distribution functions  $q(x, Q^2)$  indicated in the curly brackets:

$$F_2^{W^+ N_0(A)}(x, Q^2) = F_1^{W^+ N_0(A)}(x, Q^2) \{ Q^{N_0(A)}(x, Q^2) \rightarrow 2xq^{N_0(A)}(x, Q^2), q^{N_0(A)}(\xi_k, Q^2) \rightarrow 2\xi_k q^{N_0(A)}(\xi_k, Q^2) \}, \quad (34)$$

$$F_3^{W^+ N_0(A)}(x, Q^2) = 2F_1^{W^+ N_0(A)}(x, Q^2) \{ \bar{q}^{N_0(A)}(x, Q^2) \rightarrow -\bar{q}^{N_0(A)}(x, Q^2) \}. \quad (35)$$

There are similar formulas for the  $W^-$ -current exchange reaction.

## B. The values of the parameters

In the last section we presented the formulas involved in our formalism. We shall take the value for most of the parameters to be the same as those in Ref. [32]. The values of other parameters are chosen in order to fit the experimental data [44–46] on  $F_2^{N_0}$ ,  $(F_2^p - F_2^n)$ ,  $F_2^n/F_2^p$  they are then checked against the known nuclear shadowing and antishadowing effects [47,48]. A summary of the set of parameters is given in Table I.

With the above parameters, the average nucleon structure function

$$F_2 = F_2^{N_0} = \frac{F_2^p + F_2^n}{2} \quad (36)$$

for the photon exchange case are shown as a solid curve in Fig. 4. The valence and sea contributions to  $F_2$  are also presented as dashed and dotted curves in Fig. 4.  $F_2$  is close to the Stanford Linear Accelerator Center (SLAC) and New Muon Collaboration (NMC) [46] experimental data. We also show our results of the difference  $F_2^p - F_2^n$  and the ratio  $F_2^n/F_2^p$  of the nucleon structure functions in Fig. 5 and Fig. 6, respectively. In the coming subsection we will show the nuclear effects on the structure functions and in the next section estimate the nuclear shadowing and antishadowing effects on the extraction of  $\sin^2 \theta_W$ .

## C. Nuclear shadowing and antishadowing effects

We introduce the ratio

$$R = F_2^A/F_2^{N_0} \quad (37)$$

to indicate the nuclear electromagnetic shadowing and antishadowing effect. We will focus on the nucleus  $^{56}\text{Fe}$  since an iron target was used in the NuTeV experiment and test the nuclear effect in the  $x > 0.01$  region since 97% of the NuTeV data is from  $0.01 < x < 0.75$  [49]. In Figs. 7 and 8, we show the quark  $q$  and antiquark  $\bar{q}$  contributions to the ratio of the structure functions. In order to stress the

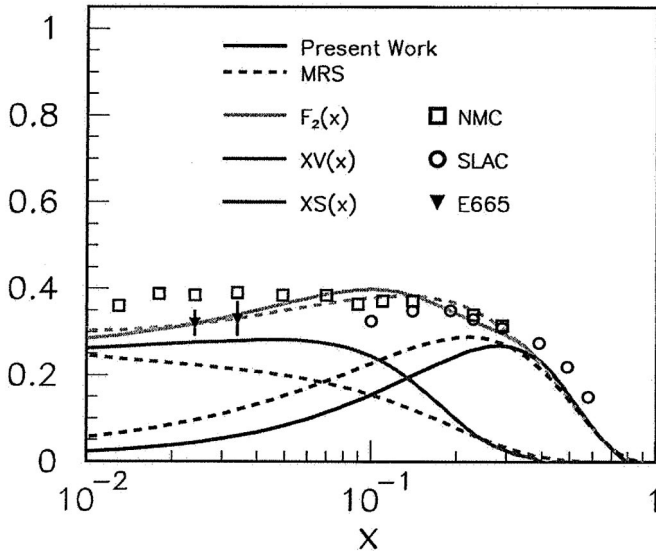


FIG. 4. The calculated nucleon structure function (biggest solid curve), valence (next solid curve at large  $x$  values), and sea (smallest solid curve at large  $x$  values) contributions to  $F_2$ , and the corresponding result of the MRST parametrization [43] (dashed curves), at  $Q^2 = 1 \text{ GeV}^2$ . The experimental data are taken from Ref. [46].

individual contribution of quarks, the numerator of the ratio  $F_2^A/F_2^{N_0}$  shown in these two figures is obtained from the denominator by a replacement  $q^{N_0}(\bar{q}^{N_0})$  into  $q^A(\bar{q}^A)$  for only the considered quark (antiquark). Because the strange quark distribution is much smaller than  $u$  and  $d$  quark distributions, the strange quark contribution to the ratio is very close to 1 although  $s^A/s^{N_0}$  may significantly deviate from 1.

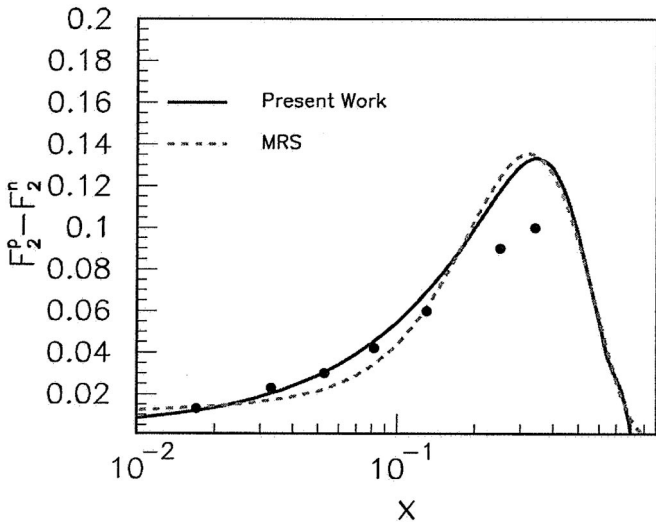


FIG. 5. The calculated difference  $F_2^p - F_2^n$  of the nucleon structure functions (solid curve) and the corresponding result of the MRST parametrization [43] (dashed curve), at  $Q^2 = 1 \text{ GeV}^2$ . The experimental data are taken from Ref. [45].

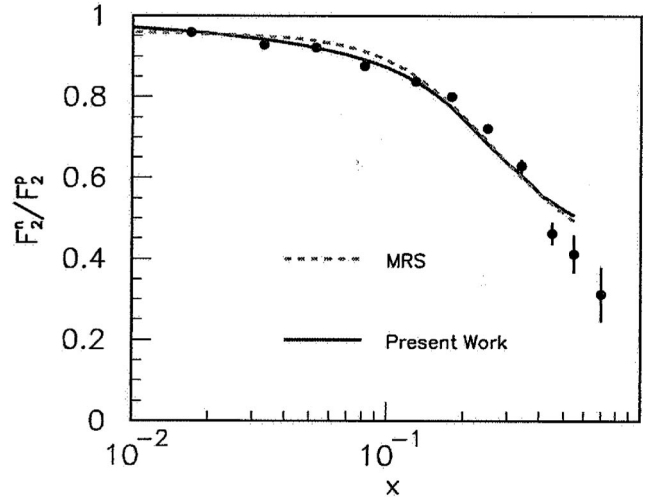


FIG. 6. The calculated ratio  $F_2^n/F_2^p$  of the nucleon structure functions (solid curve) and the corresponding result of the MRST parametrization [43] at energy scale 1 GeV (dashed curve). The experimental data are taken from Ref. [45].

In Fig. 9, we give our prediction of the nuclear shadowing and antishadowing effects (the sum of all quark and antiquark contributions to the ratio  $R$ ) for nuclei  $^{56}\text{Fe}$  and  $^{40}\text{Ca}$ . From Fig. 9, we find that our model can explain well

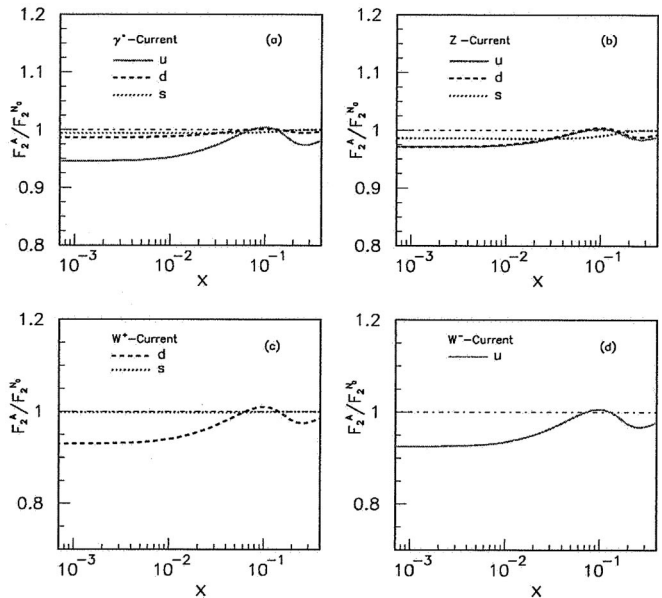


FIG. 7. The quark contributions to the ratios of structure functions at  $Q^2 = 1 \text{ GeV}^2$ , for  $\gamma^*$ ,  $Z$ ,  $W^+$ , and  $W^-$  currents [figures (a), (b), (c), (d), respectively]. The solid, dashed, and dotted curves correspond to the  $u$ ,  $d$ , and  $s$  quark contributions, respectively. This corresponds in our model to the nuclear dependence of the  $\sigma(\bar{u} - A)$ ,  $\sigma(\bar{d} - A)$ ,  $\sigma(\bar{s} - A)$  cross sections, respectively. In order to stress the individual contribution of quarks, the numerator of the ratio  $F_2^A/F_2^{N_0}$  shown in these two figures is obtained from the denominator by a replacement  $q^{N_0}$  into  $q^A$  for only the considered quark. As a result, the effect of antishadowing appears diminished.

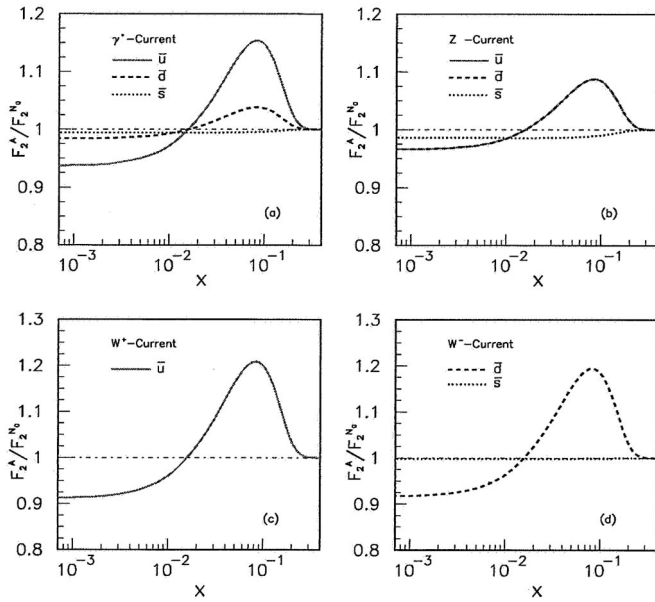


FIG. 8. The antiquark contributions to ratios of the structure functions at  $Q^2 = 1 \text{ GeV}^2$ , for  $\gamma^*$ ,  $Z$ ,  $W^+$ , and  $W^-$  currents [figures (a), (b), (c), (d), respectively]. The solid, dashed, and dotted curves correspond to  $\bar{u}$ ,  $\bar{d}$ , and  $\bar{s}$  quark contributions, respectively. This corresponds in our model to the nuclear dependence of the  $\sigma(u - A)$ ,  $\sigma(d - A)$ ,  $\sigma(s - A)$  cross sections, respectively. In order to stress the individual contribution of quarks, the numerator of the ratio  $F_2^A/F_2^{N_0}$  shown in these two figures is obtained from the denominator by a replacement  $\bar{q}^{N_0}$  into  $\bar{q}^A$  for only the considered antiquark.

the experimental data on the nuclear shadowing and antishadowing effect in DIS for electromagnetic currents.

We can further check our model by predicting the ratio of  $F_2$  structure functions  $F_{2A}[\text{neutrino}]/$

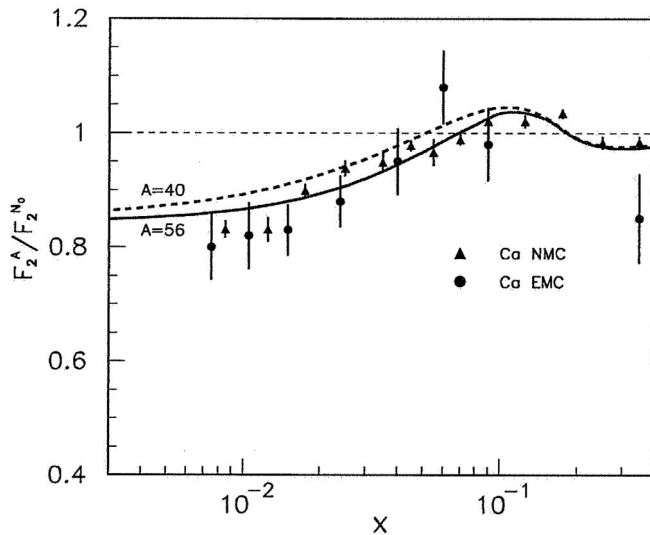


FIG. 9. The nuclear shadowing and antishadowing effects at  $\langle Q^2 \rangle = 1 \text{ GeV}^2$ . The experimental data are taken from Refs. [47,48].

$(18/5)F_{2A}[\text{muon}]$ , which has been measured by the NuTeV collaboration [50]. The results are shown in Fig. 10, and they agree very well with the experimental data, in a calculation with no further free parameters. Notice that the data for the ratio tends to go below 1 for  $x > 0.4$ , which is also what we find. In this case we have taken  $Q^2 = 20 \text{ GeV}^2$ , which is the average value of the NuTeV experiment.

We emphasize that the nuclear shadowing and antishadowing of the different currents are not universal since they depend on the different quark species. We still have factorization in the sense that we will have the same shadowing quark by quark in nuclear Drell-Yan processes.

In the case of weak currents, the shadowing/antishadowing effects are strongly influenced by the behavior of the structure function  $F_3$ , which is not present in the electromagnetic case. We will present in the next section cross section ratios (nucleus/nucleon) to illustrate the shadowing/antishadowing effects in weak current interactions.

### III. NUCLEAR EFFECTS ON EXTRACTION OF $\sin^2\theta_W$

The observables measured in neutrino DIS experiments are the ratios of NC to CC current events; these are related via Monte Carlo simulations to  $\sin^2\theta_W$ . In order to examine the possible impact of nuclear shadowing and antishadowing corrections on the extraction of  $\sin^2\theta_W$ , one is usually interested in the following ratios

$$R_A^\nu = \frac{\sigma(\nu_\mu + A \rightarrow \nu_\mu + X)}{\sigma(\nu_\mu + A \rightarrow \mu^- + X)}, \quad (38)$$

$$R_A^{\bar{\nu}} = \frac{\sigma(\bar{\nu}_\mu + A \rightarrow \bar{\nu}_\mu + X)}{\sigma(\bar{\nu}_\mu + A \rightarrow \mu^+ + X)}, \quad (39)$$

of NC to CC neutrino (antineutrino) cross sections for a nuclear target  $A$ . As is well known, if nuclear effects are neglected for an isoscalar target, one can extract the

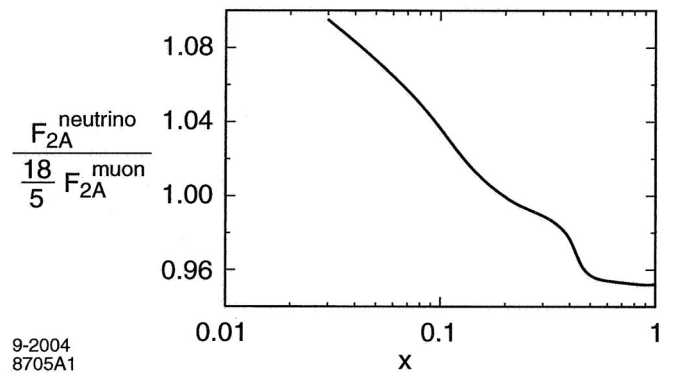


FIG. 10. Our predictions for the ratio of  $F_2$  structure functions  $F_{2A}[\text{neutrino}]/(18/5)F_{2A}[\text{muon}]$ , measured in Ref. [50], at  $Q^2 = 20 \text{ GeV}^2$ .

weak-mixing angle by using the Llewellyn-Smith relation [51]:

$$R_N^{\nu|\bar{\nu}|} = \frac{\sigma(\nu_\mu[\bar{\nu}_\mu] + N \rightarrow \nu_\mu[\bar{\nu}_\mu] + X)}{\sigma(\nu_\mu[\bar{\nu}_\mu] + N \rightarrow \mu^-[\mu^+] + X)} \\ = \rho_0^2 \left[ \frac{1}{2} - \sin^2\theta_W + \frac{5}{9} \sin^4\theta_W (1 + r^{[-1]}) \right], \quad (40)$$

written in terms of NC and CC (anti)neutrino-nucleon cross sections. Here

$$\rho_0 = \frac{M_W^2}{\cos^2\theta_W M_Z^2}, \quad r = \frac{\sigma(\bar{\nu}_\mu + N \rightarrow \mu^+ + X)}{\sigma(\nu_\mu + N \rightarrow \mu^- + X)} \sim \frac{1}{2}. \quad (41)$$

However, actual targets such as the iron target of the NuTeV experiment are not always isoscalar, having a significant neutron excess. In addition, as we have stressed here, nuclear effects due to multiscattering could be very important. These nuclear effects should also modify the CC and NC structure functions, and therefore a detailed study of these effects on the extraction of the weak-mixing angle is essential. In order to reduce the uncertainties related to sea quarks, Paschos and Wolfenstein [52] showed that one can extract  $\sin^2\theta_W$  from the relationship

$$R_N^- = \frac{\sigma(\nu_\mu + N \rightarrow \nu_\mu + X) - \sigma(\bar{\nu}_\mu + N \rightarrow \bar{\nu}_\mu + X)}{\sigma(\nu_\mu + N \rightarrow \mu^- + X) - \sigma(\bar{\nu}_\mu + N \rightarrow \mu^+ + X)} \\ = \rho_0^2 \left( \frac{1}{2} - \sin^2\theta_W \right). \quad (42)$$

Inspired by the above relation, we will examine nuclear effects on  $\sin^2\theta_W$  by the following observable for the scattering of a nuclear target  $A$ ,

$$R_A^- = \frac{\sigma(\nu_\mu + A \rightarrow \nu_\mu + X) - \sigma(\bar{\nu}_\mu + A \rightarrow \bar{\nu}_\mu + X)}{\sigma(\nu_\mu + A \rightarrow \mu^- + X) - \sigma(\bar{\nu}_\mu + A \rightarrow \mu^+ + X)}. \quad (43)$$

In the previous section, we have shown in Fig. 9 the nuclear effect on the electromagnetic structure functions. Here we can also look at the nuclear effect on the cross sections in CC and NC neutrino-nucleus DIS. If Fig. 11, we show ratios  $F_2^A/F_2^{N_0}$  (solid curves) and  $F_3^A/F_3^{N_0}$  (dashed curves) for various current exchange interactions. The fact that the  $F_3^A/F_3^{N_0}$  ratio for the  $W^-$ -current becomes negative and divergent for small  $x$  comes from the behavior of  $F_2^{N_0}$ , which in our model vanishes for  $x \sim 0.01$ . In addition, we are interested in the following ratios

$$R_Z^\nu(x) = \frac{d\sigma(\nu_\mu + A \rightarrow \nu_\mu + X)/dx}{d\sigma(\nu_\mu + N \rightarrow \nu_\mu + X)/dx}, \quad (44)$$

$$R_Z^{\bar{\nu}}(x) = \frac{d\sigma(\bar{\nu}_\mu + A \rightarrow \bar{\nu}_\mu + X)/dx}{d\sigma(\bar{\nu}_\mu + N \rightarrow \bar{\nu}_\mu + X)/dx}, \quad (45)$$

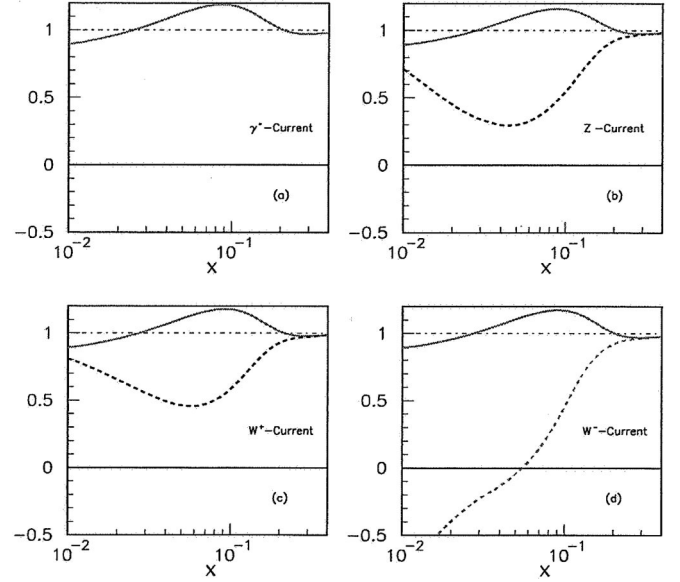


FIG. 11. Ratios  $F_2^A/F_2^{N_0}$  (solid curves) and  $F_3^A/F_3^{N_0}$  (dashed curves) for  $\gamma^*$ ,  $Z$ ,  $W^+$ , and  $W^-$  current exchange interactions [figures (a), (b), (c), (d), respectively], at  $Q^2 = 1 \text{ GeV}^2$ .

$$R_W^\nu(x) = \frac{d\sigma(\nu_\mu + A \rightarrow \mu^- + X)/dx}{d\sigma(\nu_\mu + N \rightarrow \mu^- + X)/dx}, \quad (46)$$

$$R_W^{\bar{\nu}}(x) = \frac{d\sigma(\bar{\nu}_\mu + A \rightarrow \mu^+ + X)/dx}{d\sigma(\bar{\nu}_\mu + N \rightarrow \mu^+ + X)/dx}. \quad (47)$$

The above ratios are closely related to the nuclear effects in the ratio

$$R_{A/N}^- = R_A^-/R_N^-, \quad (48)$$

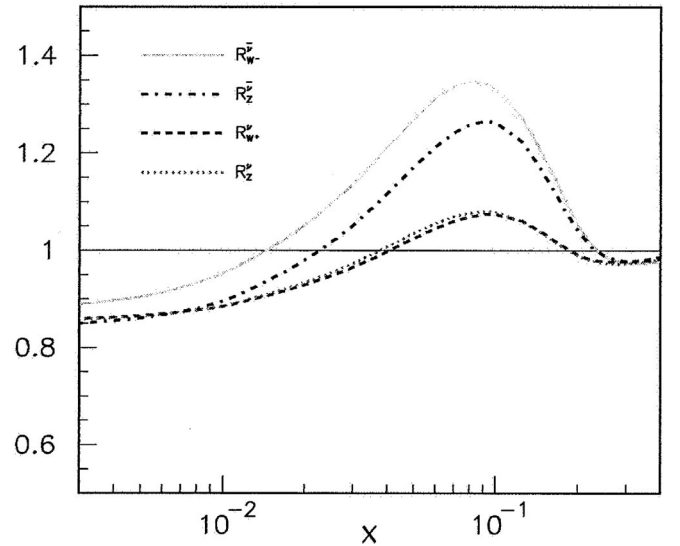


FIG. 12. The nuclear effect on the cross sections of CC and NC neutrino-nucleus DIS, at  $Q^2 = 1 \text{ GeV}^2$ . The dotted and dashed curves almost overlap.

which are later used to extract the nuclear effect on the weak-mixing angle. In Fig. 12, we show the ratios of Eqs. (44)–(47). From Figs. 9–12, one finds that the nuclear effect for charged and neutral currents is substantially different from that for the electromagnetic nuclear structure functions. There is a strong antishadowing effect in  $R_Z^\nu$  and  $R_{W^-}^\nu$ , but there is a small one in  $R_Z^\nu$  and  $R_{W^+}^\nu$ . Moreover, for neutrinos the NC and CC shadowing/antishadowing effects are the same, but for antineutrinos they are substantially different. As a result, in the neutrino case the Llewellyn-Smith relation can be used in order to extract the weak-mixing angle, but it cannot be used for this purpose in the case of antineutrino deep inelastic scattering in nuclei.

If the nuclear target had zero isospin and there was no contribution from  $s$  or  $\bar{s}$  quarks, then there would be no nuclear correction to the Llewellyn-Smith relation. However, when one includes the strange quark currents, the situation is different. The neutral current interactions of the antineutrino on the  $\bar{s}$  are shadowed rather than antishadowed (see Fig. 11) in the region  $x \sim 0.1$ , which reduces the total antishadowing effect. The charged current interactions of the antineutrino still experience strong antishadowing from the  $\bar{d}$ . In contrast, neutrino interactions are relatively insensitive to the strange quark current since they are dominated by interactions on the valence quarks, not the antiquarks. Even when one includes the strange quarks, antineutrino NC and CC interactions experience more antishadowing than neutrinos (see Fig. 12).

An alternative way of assessing the nuclear corrections is through a modified Paschos-Wolfenstein ratio  $R_A^-(x)/R_N^-(x)$ , in which instead of the total cross section we consider the corresponding differential cross sections, as shown in Fig. 13. In this case we have taken  $Q^2 = 20 \text{ GeV}^2$ , which is the average value of the NuTeV experiment.

In our numerical analysis we studied the influence of nuclear effects on the extraction of  $\sin^2\theta_W$  from the observable  $R_A^-$ , taking into account some kinematical cut-offs specific to the NuTeV experiment.

The differential cross sections for CC and NC (anti)neutrino-nucleus deep inelastic scattering are given by [53]

$$\begin{aligned} \frac{d^2\sigma_{CC}^{\nu,\bar{\nu}(A)}}{dxdy} &= \frac{G_F^2}{\pi} m_N E_{\nu,\bar{\nu}} \left\{ xy^2 F_1^{W^\pm(A)}(x, Q^2) \right. \\ &+ \left( 1 - y - \frac{xy m_N}{2E_{\nu,\bar{\nu}}} \right) F_2^{W^\pm(A)}(x, Q^2) \\ &\left. \pm \left( y - \frac{y^2}{2} \right) x F_3^{W^\pm(A)}(x, Q^2) \right\}, \end{aligned} \quad (49)$$

for the CC reaction, and

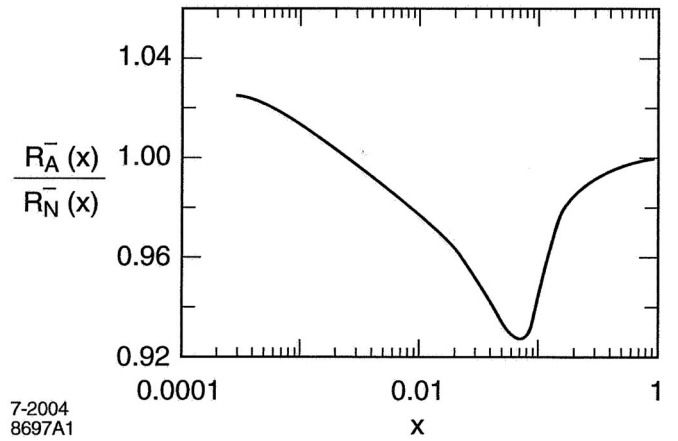


FIG. 13. The nuclear effect on the Paschos-Wolfenstein ratio of differential cross sections  $R_A^-(x)/R_N^-(x)$ , at  $Q^2 = 20 \text{ GeV}^2$ .

$$\begin{aligned} \frac{d^2\sigma_{NC}^{\nu,\bar{\nu}(A)}}{dxdy} &= \frac{G_F^2}{\pi} m_N E_{\nu,\bar{\nu}} \left\{ xy^2 F_1^{Z(A)}(x, Q^2) \right. \\ &+ \left( 1 - y - \frac{xy m_N}{2E_{\nu,\bar{\nu}}} \right) F_2^{Z(A)}(x, Q^2) \\ &\left. \pm \left( y - \frac{y^2}{2} \right) x F_3^{Z(A)}(x, Q^2) \right\}, \end{aligned} \quad (50)$$

for the NC reaction.

In the event selection, the NuTeV Collaboration applied the cutoff

$$20 \text{ GeV} \leq E_{\text{cal}} \leq 180 \text{ GeV}, \quad (51)$$

for a visible energy deposit to the calorimeter  $E_{\text{cal}}$ . The lower limit ensures full efficiency of the trigger, allows for an accurate vertex determination and reduces cosmic ray background.

Therefore we will calculate the observables  $R_S^{\nu(\bar{\nu})}$  and  $R_A^-$  imposing the same cutoff on the energy  $E_h$  of the final hadronic state  $X$  assuming  $E_h = E_{\text{cal}}$ . Since  $E_h \approx \nu$ , we can write the kinematical variables averaged over the (anti)neutrino flux as

$$x = \frac{Q^2}{2M_N E_{\text{cal}}} \leq 1, \quad y = \frac{E_{\text{cal}}}{\langle E_{\nu(\bar{\nu})} \rangle} \leq 1. \quad (52)$$

For the average energies of the neutrino and antineutrino beams we take the values  $\langle E_\nu \rangle = 120 \text{ GeV}$  and  $\langle E_{\bar{\nu}} \rangle = 112 \text{ GeV}$ , as in the NuTeV experiment [54].

We will assume a modified version of the Paschos-Wolfenstein relation:

$$\begin{aligned} R_N^-(\sin^2\theta_W) &= \rho_0^2(1 + \varepsilon) \left( \frac{1}{2} - \sin^2\theta_W \right) \\ &= \rho^2 \left( \frac{1}{2} - \sin^2\theta_W \right), \end{aligned} \quad (53)$$

where,  $\rho^2 = \rho_0^2(1 + \varepsilon)$  with a modified factor  $(1 + \varepsilon)$  due to strange quark, isospin breaking, threshold corrections for heavy quarks production, and so on. We further as-

sume that the Paschos-Wolfenstein relation can be applied to the scattering on a nuclear target  $A$ ,

$$R_A^-(\sin^2\theta_W) = \rho^2 \left[ \frac{1}{2} - (\sin^2\theta_W + \Delta\sin^2\theta_W) \right], \quad (54)$$

with a correction  $\Delta\sin^2\theta_W$  to the weak-mixing angle. In Fig. 14(a), we show the  $\sin^2\theta_W$  dependence in the ratio  $R_{A/N}^-$ . We estimate  $\Delta\sin^2\theta_W$  in the following way. First, we use the cross sections to calculate the Paschos-Wolfenstein ratios  $R_A^-(\sin^2\theta_W)$  and  $R_N^-(\sin^2\theta_W)$  with various values of  $\sin^2\theta_W$ . Second, we extract  $\rho^2$  by means of Eq. (53). In principle,  $\rho^2$  should be different for various values of  $\sin^2\theta_W$ . We find a weak dependence of  $\rho^2$  on  $\sin^2\theta_W$  and  $\rho^2 \approx 1.04$ . Finally, we use the obtained  $\rho^2$  to extract the shadowing/antishadowing effect on the weak-mixing angle  $\Delta\sin^2\theta_W$  from Eq. (54). The results are given in Fig. 14(b).

We have performed a numerical calculation at the average  $\langle Q^2 \rangle = 20 \text{ GeV}^2$  of the NuTeV experiment and have found that the modification to the weak-mixing angle is approximately  $\delta\sin^2\theta_W = 0.001$ . The value of  $\sin^2\theta_W$  determined from the NuTeV experiment, without including nuclear shadowing/antishadowing due to multiple scattering, is in absolute value 0.005 larger than the best value obtained from other experiments. The model used here to compute nuclear shadowing/antishadowing effect would reduce the discrepancy between the neutrino and electromagnetic measurements of  $\sin^2\theta_W$  by about 20%. Together with the charge symmetry violation contributions to the neutrino reactions [55], about half of the difference between the standard model and the NuTeV result can be accounted for. We also note that the antishadowing effects we predict are most important in the antineutrino data, which is less sensitive to  $\sin^2\theta_W$ .

**IV. CONCLUSIONS**

We have investigated nuclear shadowing and antishadowing effects arising from the multiple scattering of quarks and antiquarks in the nucleus. The effective quark-nucleon scattering amplitude includes Pomeron and Odderon contributions from multigluon exchange as

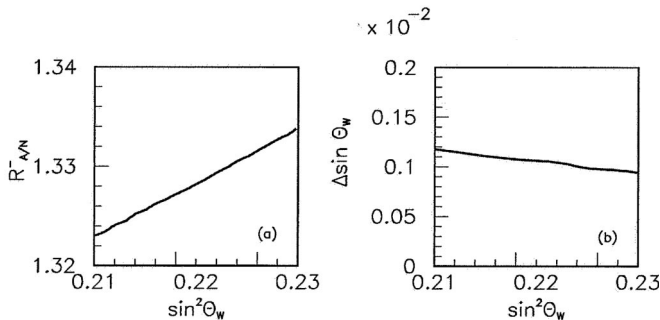
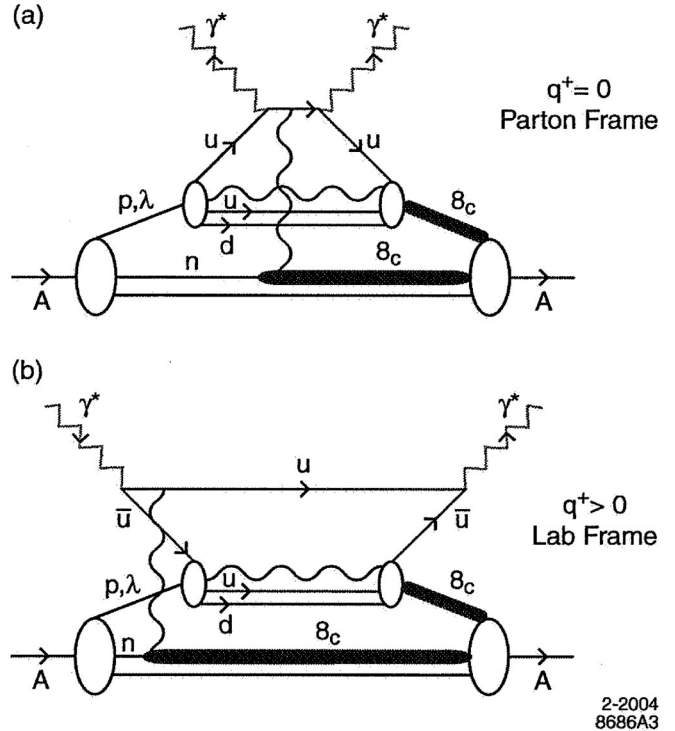


FIG. 14. (a) The  $\sin^2\theta_W$  dependence in  $R_{A/N}^-$ ; (b) The nuclear shadowing/antishadowing corrections to the  $\sin^2\theta_W$ .

well as Reggeon quark-exchange contributions. The model is constrained by measurements of the nuclear structure functions in deep inelastic electron and muon scattering as well as the Regge behavior of the nonsinglet structure functions. We have also noted the possibility of obtaining an antishadowing contribution from one-gluon exchange  $\times$  Reggeon exchange, assuming the existence of hidden-color components in the nuclear wave function. We have shown that the coherence of these multiscattering nuclear processes leads to shadowing and antishadowing of the electromagnetic nuclear structure functions in agreement with measurements. The momentum sum rule is not satisfied in a nuclear target by balancing the shad-



2-2004  
8686A3

FIG. 15. Representation of leading-twist QCD “hidden-color” contributions to the nuclear structure function from the absorptive part of the forward virtual Compton amplitude  $ImT(\gamma^*A \rightarrow \gamma^*A)$ . (a) Illustration of a two-step contribution in the  $q^+ = 0$ ,  $q_{\perp}^2 = Q^2$  parton model frame—deep inelastic lepton scattering on a valence quark of a target proton followed by the final-state single-gluon interaction of the outgoing quark on a target neutron. The proton and neutron are both color excited to color-octet states. The amplitude requires the presence of hidden-color components in the nuclear wave function. (b) Illustration of the physics of the two-step process shown in (a), but in the laboratory frame where  $q^+ > 0$ . The  $u\bar{u}$  fluctuation of the virtual photon first scatters via a single-gluon exchange on a neutron; this is then followed by the annihilation of the  $\bar{u}$  quark on a proton. The proton and neutron are both color excited to color-octet states. The amplitude requires the presence of hidden-color components in the nuclear wave function. The two-step annihilation amplitude on the proton alone, thus producing antishadowing. Similar processes occur in the case of the weak currents.

owing and antishadowing of the leading-twist nuclear quark distributions; however the momentum sum rule can still be satisfied if there is a compensating change in the nuclear gluon distribution.

Our analysis leads to substantially different nuclear antishadowing for charged and neutral current reactions; in fact, the neutrino and antineutrino DIS cross sections are each modified in different ways due to the various allowed Regge exchanges. The nonuniversality of nuclear effects will modify the extraction of the weak-mixing angle  $\sin^2\theta_W$ , particularly because of the strong nuclear effects for the  $F_3$  structure function. The shadowing and antishadowing of the strange quark structure function in the nucleus can also be considerably different than that of the light quarks. We thus find that part of the anomalous NuTeV result for  $\sin^2\theta_W$  could be due to the nonuniversality of nuclear antishadowing for charged and neutral currents. Our picture also implies nonuniversality for the nuclear modifications of spin-dependent structure functions.

We have found in our analysis that the antishadowing of nuclear structure functions depends in detail on quark flavor. Careful measurements of the nuclear dependence of charged, neutral, and electromagnetic DIS processes are thus needed to establish the distinctive phenomenology of shadowing and antishadowing and to make the NuTeV results definitive. It is also important to map out the shadowing and antishadowing of each quark component of the nuclear structure functions to illuminate the underlying QCD mechanisms. Such studies can be carried out in semi-inclusive deep inelastic scattering for the electromagnetic current at Hermes and at Jefferson Laboratory by tagging the flavor of the current quark or by using pion and kaon-induced Drell-Yan reactions. A new determination of  $\sin^2\theta_W$  is also expected from the neutrino scattering experiment NOMAD at CERN [56]. A systematic program of measurements of the nuclear effects in charged and neutral current reactions could also be carried out in high-energy electron-nucleus colliders such as HERA and eRHIC, or by using high intensity neutrino beams [57].

### ACKNOWLEDGMENTS

We thank Stefan Kretzer, Kevin McFarlane, and Paul Hoyer for helpful comments, and Alfonso Zerwekh for

assistance with the numerical analysis. Work was supported in part by the Department of Energy under Contract No. DE-AC03-76SF00515, by the Foundation for University Key Teacher by the Ministry of Education (China), by Fondecyt (Chile) Grant No. 1030355, and by the National Natural Science Foundation of China under Grant No. 19875024 and No. 10025523.

### APPENDIX: A NON-ABELIAN SOURCE FOR ANTISHADOWING

We can identify a further antishadowing contribution specific to the non-Abelian theory. Consider once again Fig. 2 for  $\gamma^*A \rightarrow \gamma^*A$ , but replace the two exchanged gluons with just a single-gluon (see Fig. 15). For simplicity we display the case of a deuteron target. In Fig. 4 the exchanged gluon attaches to the struck  $u$  quark valence constituent of the proton at the top of the diagram changing its color. This also changes the scattered proton  $p'$  to a color octet. The exchange gluon also transforms the spectator neutron into a color octet. Thus if the deuteron wave function contains hidden-color  $|8_C 8_C\rangle$  components, this process interferes with the one-step diagram with no final-state interactions.

The deuteron certainly has hidden-color components—one only has to exchange a gluon between the nucleons in the deuteron light-front wave function (LFWF) [58]. The large magnitude of the deuteron form factor also demands hidden-color components [59]. The calculation of the one-gluon exchange effects is very similar to our Odderon analysis. The one-gluon exchange amplitude behaves as  $s^1$  and a nearly real phase. Like the Odderon, it has  $C = -$  and couples with opposite sign to the  $q$  and  $\bar{q}$ . A complication is how to understand the Reggeon exchange amplitude on the proton since the  $u$  and  $\bar{u}$  in the  $t$  channel now are in a color-octet configuration. Nevertheless, the Odderon calculation serves as a model for the one-gluon exchange contribution and its effect on antishadowing.<sup>2</sup>

<sup>2</sup>A modification to the usual Glauber approximation through a possible Pomeron color structure has also been considered in Ref. [60].

- [1] ALEPH Collaboration, D. Abbaneo *et al.*, hep-ex/0112021.  
 [2] NuTeV Collaboration, G. P. Zeller *et al.*, Phys. Rev. Lett. **88**, 091802 (2002); **90**, 239902(E) (2003).

- [3] SLAC E158 Collaboration, P. L. Anthony *et al.*, Phys. Rev. Lett. **92**, 181602 (2004).  
 [4] M. Burkardt and B. Warr, Phys. Rev. D **45**, 958 (1992).  
 [5] S. J. Brodsky and B. Q. Ma, Phys. Lett. B **381**, 317 (1996).

- [6] S. Kovalenko, I. Schmidt, and J. J. Yang, *Phys. Lett. B* **546**, 68 (2002).
- [7] G. A. Miller and A. W. Thomas, hep-ex/0204007 [Int. J. Mod. Phys. E (to be published)].
- [8] NuTeV Collaboration, G. P. Zeller *et al.*, hep-ex/0207052.
- [9] NuTeV Collaboration, G. P. Zeller *et al.*, *Phys. Rev. D* **65**, 111103 (2002); **67**, 119902(E) (2003).
- [10] K. S. McFarland *et al.*, *Int. J. Mod. Phys. A* **18**, 3841 (2003).
- [11] K. P. O. Diener, S. Dirrmaier, and W. Hollik, *Phys. Rev. D* **69**, 073005 (2004).
- [12] S. A. Kulagin, *Phys. Rev. D* **67**, 091301 (2003).
- [13] NuTeV Collaboration, R. H. Bernstein, *J. Phys. G* **29**, 1919 (2003).
- [14] S. Kretzer, hep-ph/0405221.
- [15] S. Kretzer *et al.*, *Phys. Rev. Lett.* **93**, 041802 (2004).
- [16] S. Davidson *et al.*, *J. High Energy Phys.* 02 (2002) 037.
- [17] R. J. Glauber, *Phys. Rev.* **100**, 242 (1955).
- [18] V. N. Gribov, *Zh. Eksp. Teor. Fiz.* **57**, 1306 (1969) [*Sov. Phys. JETP* **30**, 709 (1970)].
- [19] L. Stodolsky, *Phys. Rev. Lett.* **18**, 135 (1967).
- [20] S. J. Brodsky and J. Pumplin, *Phys. Rev.* **182**, 1794 (1969).
- [21] B. L. Ioffe, *Phys. Lett. B* **30**, 123 (1969).
- [22] L. L. Frankfurt and M. I. Strikman, *Nucl. Phys.* **B316**, 340 (1987).
- [23] B. Z. Kopeliovich, J. Raufeisen, and A. V. Tarasov, *Phys. Lett. B* **440**, 151 (1998).
- [24] D. E. Kharzeev and J. Raufeisen, nucl-th/0206073, and references therein.
- [25] A. H. Mueller and A. I. Shoshi, *Nucl. Phys. B* **692**, 175 (2004).
- [26] J. W. Qiu and I. Vitev, hep-ph/0405068.
- [27] A. D. Marin, M. G. Ryskin, and G. Watt, *Eur. Phys. J. C* **37**, 285 (2004).
- [28] H1 Collaboration, C. Adloff *et al.*, *Z. Phys. C* **76**, 613 (1997).
- [29] M. Ruspa, *Acta Phys. Pol. B* **35**, 473 (2004).
- [30] S. J. Brodsky *et al.*, *Phys. Rev. D* **65**, 114025 (2002).
- [31] S. J. Brodsky, D. S. Hwang, and I. Schmidt, *Phys. Lett. B* **530**, 99 (2002).
- [32] S. J. Brodsky and H. J. Lu, *Phys. Rev. Lett.* **64**, 1342 (1990).
- [33] J. Kuti and V. F. Weisskopf, *Phys. Rev. D* **4**, 3418 (1971).
- [34] M. Arneodo, *Phys. Rep.* **240**, 301 (1994).
- [35] C. Ewerz, hep-ph/0306137; See also H. G. Dosch, C. Ewerz, and V. Schatz, *Eur. Phys. J. C* **24**, 561 (2002).
- [36] J. Bartels, L. N. Lipatov, and G. P. Vacca, *Phys. Lett. B* **477**, 178 (2000).
- [37] P. V. Landshoff, J. C. Polkinghorne, and R. D. Short, *Nucl. Phys. B* **28**, 225 (1971).
- [38] S. J. Brodsky, F. E. Close, and J. F. Gunion, *Phys. Rev. D* **8**, 3678 (1973).
- [39] L. L. Frankfurt and M. I. Strikman, *Nucl. Phys. B* **316**, 340 (1988); *Phys. Rep.* **160**, 235 (1988).
- [40] P. D. B. Collins, *An Introduction to Regge Theory and High Energy Physics* (Cambridge University Press, Cambridge, England, 1977).
- [41] V. Barone, C. Pascaud, and F. Zomer, *Eur. Phys. J.* **C12**, 243 (2000).
- [42] CTEQ Collaboration, H. L. Lai *et al.*, *Eur. Phys. J.* **C12**, 375 (2000).
- [43] A. D. Martin *et al.*, University of Durham Report No. DTP/99/64, 1999 (to be published).
- [44] New Muon Collaboration, M. Arneodo *et al.*, *Nucl. Phys. B* **481**, 23 (1996).
- [45] New Muon Collaboration, P. Amaudruz *et al.*, *Phys. Rev. Lett.* **66**, 2712 (1991).
- [46] Particle Data Group Collaboration, S. Eidelman *et al.*, *Phys. Lett. B* **592**, 1 (2004).
- [47] EMC-NA28 Collaboration, M. Arneodo *et al.*, *Nucl. Phys. B* **333**, 1 (1990).
- [48] NMC Collaboration, P. Amaudruz *et al.*, *Z. Phys. C* **51**, 387 (1991).
- [49] K. S. McFarland *et al.*, *Nucl. Phys. B, Proc. Suppl.* **112**, 226 (2002).
- [50] CCFR/NuTeV Collaboration, U. K. Yang *et al.*, *Phys. Rev. Lett.* **86**, 2742 (2001).
- [51] C. H. Llewellyn-Smith, *Nucl. Phys. B* **228**, 205 (1983).
- [52] E. A. Paschos and L. Wolfenstein, *Phys. Rev. D* **7**, 91 (1973).
- [53] E. Leader and E. Predazzi, *An Introduction to Gauge Theories and the New Physics* (Cambridge University Press, Cambridge, England, 1983).
- [54] G. P. Zeller (private communication).
- [55] J. T. Londergan and A. W. Thomas, *Phys. Lett. B* **558**, 132 (2003).
- [56] NOMAD Collaboration, R. Petti, in Proceedings of the ICHEP, 2004 (unpublished).
- [57] S. Geer, Proceedings of the Workshop on Physics with a Multi-MW Proton Source, Geneva, 2004, Report No. FERMILAB-CONF-04-133-E (unpublished).
- [58] S. J. Brodsky, C. R. Ji, and G. P. Lepage, *Phys. Rev. Lett.* **51**, 83 (1983).
- [59] G. R. Farrar, K. Huleihel, and H. Y. Zhang, *Phys. Rev. Lett.* **74**, 650 (1995).
- [60] B. Z. Kopeliovich and B. G. Zakharov, *Z. Phys. C* **26**, 459 (1984).